

COMPARATIVE ANALYSIS OF DIFFERENT NUMERICAL SCHEMES IN SOLUTE TRAPPING SIMULATIONS BY USING THE PHASE-FIELD MODEL WITH FINITE INTERFACE DISSIPATION

X. Yang^a, Y. Tang^a, D. Cai^a, L. Zhang^{a*}, Y. Du^a, S. Zhou^b

^a State Key Laboratory of Powder Metallurgy, Central South University, Changsha, Hunan, P. R. China

^b Division of Materials Sciences and Engineering, Ames Laboratory, USDOE, Ames, USA

(Received 16 July 2015; accepted 27 December 2015)

Abstract

Two different numerical schemes, the standard explicit scheme and the time-elimination relaxation one, in the framework of phase-field model with finite interface dissipation were employed to investigate the solute trapping effect in a Si-4.5 at.% As alloy during rapid solidification. With the equivalent input, a unique solute distribution under the steady state can be obtained by using the two schemes without restriction to numerical length scale and interface velocity. By adjusting interface width and interface permeability, the experimental solute segregation coefficients can be well reproduced. The comparative analysis of advantages and disadvantages in the two numerical schemes indicates that the time-elimination relaxation scheme is preferable in one-dimensional phase-field simulation, while the standard explicit scheme seems to be the only choice for two- or three dimensional phase-field simulation. Furthermore, the kinetic phase diagrams in the Si-As system were predicted by using the phase-field simulation with the time-elimination relaxation scheme.

Keywords: *Phase-field modeling; Solute trapping; Rapid solidification; Numerical scheme*

1. Introduction

Rapid solidification technology represents an important method for empowering new materials. With extremely high growth velocity, rapid solidification helps to achieve non-equilibrium microstructure, such as amorphous and quasicrystal, which show completely different properties compared with those in equilibrium or near equilibrium states [1]. During rapid solidification, the solute may be entrapped by the rapidly moving solid-liquid interface with a quantity in concentrations that differ significantly from those given by the equilibrium phase diagram. This phenomenon in rapid solidification is commonly referred as “solute trapping” [2, 3]. Solute trapping can be characterized by the velocity-dependent solute segregation coefficient $k(V)$ with V as the interface velocity. Due to its theoretical and technological importance, the feature of solute trapping has been studied extensively in the literature, not only by means of experimental investigations [4-6], but also by employing various theoretical models, such as analytical models based on a sharp interface hypothesis [7-14] or phase-field simulations based on diffusion interface models [15-23].

In the sharp-interface picture, there are two

important analytical models for describing solute trapping: (1) the continuous growth model (CGM) [7, 8] and (2) local non-equilibrium model (LNM) [9-14]. The CGM is formulated by assuming a flux balance across a moving solid-liquid interface, giving a good fit to the experimental solute segregation coefficients at low and medium interface velocities. The LNM is based on a similar approach as the CGM, but makes use of a generalized Fick's law that accounts for the finite relaxation time of the diffusion flux into its steady state. With LNM, the complete solute trapping (i.e. the solute segregation coefficient equals to 1) at finite interface velocity can be nicely predicted which means that the experimental solute segregation coefficients over the entire range of interface velocities can be well reproduced. Though these sharp-interface analytical models can nicely characterize the solute trapping phenomenon, the microstructure evolution during rapid solidification can be only simulated by using the phase-field method, which has been widely utilized to describe the non-equilibrium effect in phase transformations, and especially in rapid solidification, for the past two decades.

The phase-field model for describing the alloy solidification was first developed by Wheeler et al. [15-17], and later named as the Wheeler-Boettinger-

* Corresponding author: lijun.zhang@csu.edu.cn

McFadden (WBM) model. Based on the WBM model, Danilov and Nestler [18] developed a parabolic phase-field model, and investigated the effect of non-equilibrium solute trapping in a binary Si-As alloy during rapid solidification. The parabolic phase-field model can reproduce the experimental data at low and medium interface velocities, as does by the CGM. In order to describe the complete solute trapping at finite solidification velocity, Galenko and his co-workers [19] developed a so-called hyperbolic phase-field model by considering the inertial effects within the interface based on the WBM model. As claimed by Lebedev et al. [19], the hyperbolic phase-field model is able to predict a sharp transition to complete solute trapping, which is in good agreement with the experimental observation. However, so far, the hyperbolic phase-field model can only reproduce the complete solute trapping and experimental data with the nanometric width of the diffuse interface.

Very recently, a phase-field model with finite interface dissipation has been developed for the description of non-equilibrium phase transformations [20, 21] on a mesoscopic scale in the framework of multi-phase-field model [24-26]. At the mesoscopic scale, the concentration field, is split into the phase concentrations defined for the individual bulk phases [27]. The solute redistribution at a moving phase boundary is then considered by a local redistribution flux between the phase concentration fields which overlap at the interface. The key feature of this model is that the two concentration fields are linked by a kinetic equation which describes the exchange of the components between the phases [20], instead of an equilibrium partitioning condition. To adjust the interface dissipation in this exchange, an interface permeability, P , was introduced into the model [20]. By adjusting the interface permeability and interface width simultaneously, the experimental solute segregation coefficients can be nicely reproduced by the phase-field simulation in the length scale of micrometer [20], which provides a possibility of three-dimensional (3-D) simulation of rapid solidification in a large scale ($\sim\mu\text{m}$) [22, 23].

In order to apply the phase-field model with finite interface dissipation to simulate the solute trapping in target alloys during rapid solidification, especially for the future 3-D large-scale simulation, an appropriate numerical scheme needs to be chosen. In general, there are two numerical schemes available in the literature. The first scheme is the standard explicit scheme, which is usually adopted in the previous one-dimensional (1-D) simulations [20, 22, 23] using the phase-field model with finite interface dissipation. In the standard explicit scheme, the temporal and spatial partial differential equations are solved directly by using the classic explicit scheme. If the initial alloy composition and a temperature are given, the solute

distribution and solid-liquid interface velocity in the steady state can be predicted. The second scheme is to eliminate temporal effect in the evolution equations of phase field and concentration by introducing a reference of moving frame, $z = x - Vt$, which is moving with a constant velocity V at the centre of the interfacial zone given by $\phi = 1/2$ at $z = 0$ [18, 19]. With the input of interface velocity and initial alloy composition, the solute distribution and temperature at the front of solid-liquid interface can be predicted on the basis of the relaxation resolution [18, 19]. In order to differentiate from the standard explicit scheme, the second method is named as "the time-elimination relaxation scheme" here.

According to the previous publications [20, 22, 23], the standard explicit scheme is easily coded, but its numerical convergence to the steady state seems to be slow when the interface velocity is low or the simulation is in large-scale. While for the time-elimination relaxation scheme, its numerical convergence to the steady state is efficient, but the reliability for its application in the length scale of micrometer needs to be validated. Consequently, it is necessary to perform a comparative analysis of these two numerical schemes in the framework of phase-field model with finite interface dissipation, from which an appropriate numerical scheme is expected to be proposed for simulating solute trapping and microstructure evolution in a rapid solidified alloy. In order to achieve this goal, a Si-4.5 at.% As alloy is chosen as the target in the present work due to available experimental data in this binary alloy [6]. 1-D phase-field simulations of the solute trapping effect in Si-4.5 at.% As alloy during rapid solidification are thus performed in the present work using both standard explicit scheme and time-elimination relaxation scheme in the framework of phase-field model with finite interface dissipation.

2. Phase-field model with finite interface dissipation

According to Refs. [20, 21], a binary system with only an α - β transition can be described by the phase field ϕ_α that varies between 0 (not phase α) and 1 (phase α), its complement $\phi_\beta = 1 - \phi_\alpha$ and the overall composition c of solute As (unit: mole/cm³). The standard assumption is made that the molar volume for both phase α and β is independent of the composition and remain constant during phase transformation. In the phase-field model with finite interface dissipation, the separate phase concentration fields c_α and c_β are introduced and the overall concentration c is given by a mixture rule varying with location x and time t :

$$c(x, t) = c_\alpha(x, t)\phi_\alpha(x, t) + c_\beta(x, t)\phi_\beta(x, t) \quad (1)$$

During solidification, the total free energy F can be divided into the interfacial part f^{intf} and the chemical part f^{chem} [20]:

$$F = \int_{\Omega} \{f^{intf} + f^{chem}\} \quad (2)$$

$$f^{intf} = \frac{4\sigma_{\alpha\beta}}{\eta} \left\{ -\frac{\eta^2}{\pi^2} \nabla\phi_{\alpha} \cdot \nabla\phi_{\beta} + \phi_{\alpha}\phi_{\beta} \right\} \quad (3)$$

$$f^{chem} = \phi_{\alpha}f_{\alpha}(c_{\alpha}) + \phi_{\beta}f_{\beta}(c_{\beta}) + \lambda \{c - (\phi_{\alpha}c_{\alpha} + \phi_{\beta}c_{\beta})\} \quad (4)$$

Where η is the interface width, and $\sigma_{\alpha\beta}$ the interfacial energy. In Eq. (4), the Lagrange multiplier λ is introduced to ensure solute conservation, and its expression is proposed as [20]:

$$\lambda = \phi_{\alpha} \frac{\partial f_{\alpha}}{\partial c_{\alpha}} + \phi_{\beta} \frac{\partial f_{\beta}}{\partial c_{\beta}} - \frac{\dot{\phi}_{\alpha}c_{\alpha} + \dot{\phi}_{\beta}c_{\beta}}{P} \quad (5)$$

Where P has the dimension of an inverse action density (cm^3/Js). In fact, P is the rate constant controlling the interface dissipation, and it can be estimated as:

$$P = f(\eta) \frac{M^{inter}}{\delta_{atom}} \quad (6)$$

Where δ_{atom} is the atomic interface width, while M^{inter} is the atomic mobility over the interface as a mixture from the chemical mobility in each phase. $f(\eta)$ is a function of the numerical interface width η with the dimension [m^{-1}], and has been set to be $8/\eta$ as a first approximation in [20] and inversely with $\eta^{1.256}$ in [22], respectively.

Based on the above free energy functional, the evolution equations for phase concentrations, c_{α} and c_{β} , can be expressed as:

$$\phi_{\alpha}\dot{c}_{\alpha} = \bar{\nabla}(\phi_{\alpha}D_{\alpha}\bar{\nabla}c_{\alpha}) + P\phi_{\alpha}\phi_{\beta}\left(\frac{\partial f_{\beta}}{\partial c_{\beta}} - \frac{\partial f_{\alpha}}{\partial c_{\alpha}}\right) + \phi_{\alpha}\dot{\phi}_{\alpha}(c_{\beta} - c_{\alpha}) \quad (7)$$

$$\phi_{\beta}\dot{c}_{\beta} = \bar{\nabla}(\phi_{\beta}D_{\beta}\bar{\nabla}c_{\beta}) + P\phi_{\alpha}\phi_{\beta}\left(\frac{\partial f_{\alpha}}{\partial c_{\alpha}} - \frac{\partial f_{\beta}}{\partial c_{\beta}}\right) + \phi_{\beta}\dot{\phi}_{\beta}(c_{\alpha} - c_{\beta}) \quad (8)$$

Where D_{α} and D_{β} are the chemical diffusivities in the α and β phases, respectively, which can be experimentally measured [28, 29] or calculated from the atomic mobility databases [30, 31]. The second part in Eqs. (7) and (8) describes the flux of solute between the phases due to a difference in the diffusion potentials $\tilde{\mu}_{\alpha} = \partial f_{\alpha} / \partial c_{\alpha}$ and $\tilde{\mu}_{\beta} = \partial f_{\beta} / \partial c_{\beta}$. The third term represents the change of the phase concentrations due to phase change. In fact, the summation of Eqs. (7) and (8) gives the standard evolution equation of overall concentration, $\dot{c} = \bar{\nabla}(\phi_{\alpha}D_{\alpha}\bar{\nabla}c_{\alpha}) + \bar{\nabla}(\phi_{\beta}D_{\beta}\bar{\nabla}c_{\beta})$.

However, the nontrivial point is that this suspends the need to employ an extra condition to fix the concentrations for each phase. Instead, one can use the separated concentration evolution equations of

each phase for the iteration, which is applicable for arbitrary initial conditions, ranging from the equilibrium state to strongly non-equilibrium state.

According to Steinbach et al. [20], the evolution equation for the phase field ϕ_{α} is given by:

$$\dot{\phi}_{\alpha} = K \{ \sigma_{\alpha\beta} [\nabla^2\phi_{\alpha} + \frac{\pi^2}{\eta^2}(\phi_{\alpha} - \frac{1}{2})] - \frac{\pi}{\eta} \sqrt{\phi_{\alpha}(1-\phi_{\alpha})} \Delta g_{\alpha\beta}^{phi} \} \quad (9)$$

Where the chemical driving force, $\Delta g_{\alpha\beta}^{phi}$ is expressed as:

$$\Delta g_{\alpha\beta}^{phi} = f_{\alpha} - f_{\beta} + (\phi_{\alpha}\tilde{\mu}_{\alpha} + \phi_{\beta}\tilde{\mu}_{\beta})(c_{\beta} - c_{\alpha}) \quad (10)$$

K in Eq. (9) is a modified interface mobility given by:

$$K = \frac{8P\eta\mu_{\alpha\beta}}{8P\eta + \mu_{\alpha\beta}\pi^2(c_{\alpha} - c_{\beta})^2} \quad (11)$$

Where $\mu_{\alpha\beta}$ is the physical interface mobility.

3. Numerical schemes

3.1 Standard explicit scheme

Following the previous work [20, 22, 23], the simulations using the standard explicit numerical scheme in the framework of the phase-field model with finite interface dissipation are performed under isothermal conditions with different temperatures below or slightly above the solidus temperature of the Si-4.5 at.% As alloy. With these settings, the steady-state solidification growth can be reached during the simulation, and the interface velocity as well as the solute segregation coefficient can be determined.

In this standard explicit scheme, 1-D explicit phase-field simulations are performed by simultaneously solving the phase concentration evolution equations (7) and (8) and the phase-field evolution equation (9). The left and right boundaries for phase field are set as insulation conditions. As for the concentrations, an insulation condition is used for the left boundary, while the concentration at the right boundary is fixed at the initial alloy concentration, i.e. Si-4.5 at.% As. A moving frame is used to determine the interface velocity. The interface velocity and solute segregation coefficient vary simultaneously as the simulation temperature changes continuously. The interface permeability P is estimated to be $2.5 \times 10^4 \text{ cm}^3/(\text{Js})$ for the first simulation. In addition, the total simulation size is large enough to keep a length of 10 times the diffusion length of the liquid profile when a lower interface velocity is used.

3.2 Time-elimination relaxation scheme

The time-elimination relaxation scheme is started by introducing a reference of moving frame:

$$z = x - Vt \quad (12)$$

Table 1. Materials parameters for the phase-field simulation of the solute trapping in Si-4.5 at.% As

Parameter	Symbol	Value	Reference
Grid spacing	Δx	9.375×10^{-9} cm	present work
Interface width	η	1.875×10^{-7} cm	present work
Interface energy	σ_{LS}	4.77×10^{-5} J/cm ²	[32]
Interface mobility	μ_{LS}	2.56 cm ⁴ /Js	[20]
Chemical diffusivity of solid phase	D_S	3.0×10^{-9} cm ² /s	[6]
Chemical diffusivity of liquid phase	D_L	1.5×10^{-5} cm ² /s	[6]
Melting temperature	T_m	1685 K	[32]
Liquidus slope	m_e	-400 K/at.%	[18]
Equilibrium partitioning coefficient	k_e	0.3	[6]
Molar volume of solid/liquid phase	V_m	12 cm ³ /mol	[18]

Propagating at a constant velocity V and coincident with the center of the interface given by $\phi_\alpha = 1/2$ at $z = 0$. Eqs. (7) to (9) then become:

$$-V\phi_\alpha \frac{\partial c_\alpha}{\partial z} = \frac{\partial}{\partial z} (\phi_\alpha D_\alpha \frac{\partial c_\alpha}{\partial z}) + P\phi_\alpha \phi_\beta \left(\frac{\partial f_\beta}{\partial c_\beta} - \frac{\partial f_\alpha}{\partial c_\alpha} \right) - V\phi_\alpha (c_\beta - c_\alpha) \frac{\partial \phi_\alpha}{\partial z} \quad (13)$$

$$-V\phi_\beta \frac{\partial c_\beta}{\partial z} = \frac{\partial}{\partial z} (\phi_\beta D_\beta \frac{\partial c_\beta}{\partial z}) + P\phi_\alpha \phi_\beta \left(\frac{\partial f_\alpha}{\partial c_\alpha} - \frac{\partial f_\beta}{\partial c_\beta} \right) - V\phi_\beta (c_\alpha - c_\beta) \frac{\partial \phi_\beta}{\partial z} \quad (14)$$

$$-V \frac{\partial \phi_\alpha}{\partial z} = K \{ \sigma_{\alpha\beta} \left[\frac{\partial^2 \phi_\alpha}{\partial z^2} + \frac{\pi^2}{\eta^2} (\phi_\alpha - \frac{1}{2}) \right] - \frac{\pi}{\eta} \sqrt{\phi_\alpha (1 - \phi_\alpha)} \Delta g_{\alpha\beta}^{phi} \} \quad (15)$$

The simulation temperature is resolved by the Gibbs-Thomson equation:

$$V = \mu \{ \sigma\kappa + \Delta g \} \quad (16)$$

Where κ is the curvature term, while Δg is the chemical driving force which depends on the simulation temperature and compositions. In 1-D steady-state simulation, one can have the curvature $\kappa = 0$ and the kinetic coefficient K in the phase-field model with finite interface dissipation is used to describe the influence of finite diffusion and

redistribution on the phase transition process. Thus, equation (16) can be simplified as:

$$V = K \cdot \Delta g \quad (17)$$

The phase-field simulations using the time-elimination relaxation scheme are conducted by solving the concentration evolution equations (i.e., Eqs. (13) and (14)), the phase-field evolution equation (i.e., Eq. (15) and Eq. (17)). The initial boundary conditions for phase field and concentrations and the simulation size used in the standard explicit simulation scheme are retained in the time-elimination relaxation scheme. The spatial derivatives are discretized using finite differences on the same grid size with the explicit scheme. Starting from an initial value ($\phi_{\alpha,0}(z)$, $c_0(z)$, $c_{\alpha,0}(z)$, $c_{\beta,0}(z)$, T_0), the iterations ($\phi_{\alpha,n}(z)$, $c_n(z)$, $c_{\alpha,n}(z)$, $c_{\beta,n}(z)$, T_n) for $n \geq 1$ are computed until the convergence criteria $\|\phi_{\alpha,n} - \phi_{\alpha,n-1}\| \leq 10^{-9}$, $\|c_n - c_{n-1}\| \leq 10^{-9}c_0$, and $\|c_{\beta,n} - c_{\beta,n-1}\| \leq 10^{-9}c_{\beta,0}$ ($i = \alpha$ or β) are reached, where $\|\Psi\|$ is the L_2 -norm of the finite difference representation of a function $\Psi(z)$.

4. Solute segregation coefficient

In the phase-field model with finite interface dissipation, the individual phase concentrations are utilized and each position over the interface can be assumed to be a sharp interface. Thus, the solute segregation coefficient is defined as [20]:

$$k(V) = \frac{\text{far-field concentration}}{\text{maximum of the liquid concentration}} = \frac{c_S}{\max[c_L]} = \frac{c_S}{c_L(\phi = 0.9999)} \quad (18)$$

The far-field concentration in the liquid is equal to the concentration in the bulk solid under steady-state condition and the maximum of the liquid concentration across the interface is at the position adjacent to the solid bulk region. For simplicity, the maximum of the liquid concentration is assumed to be the liquid concentration at $\phi = 0.9999$. These concentrations can be achieved in a typical steady-state concentration profile during rapid solidification.

5. Results and discussion

Fig. 1 displays the flow chart for the comparative analysis of two numerical schemes in the present 1-D phase-field simulations of solute trapping in the Si-4.5 at.% As alloy during rapid solidification. With input of the initial phase compositions $c_{\alpha,0}$, $c_{\beta,0}$ and simulation temperature T_0 , the phase-field simulations using the standard explicit scheme were performed firstly, resulting in output of a set of interface velocity V_n , solute segregation coefficient $k_n(V)$ and solute

distribution along the entire simulation domain. With the output interface velocity V_n and the $c_{\alpha,0}$, $c_{\beta,0}$ compositions as the input, the phase-field simulations using the time-elimination relaxation scheme were then conducted. The thermophysical parameters used in both standard explicit and time-elimination relaxation schemes are listed in Table 1. With the thermophysical and numerical parameters in Table 1, the "temperature - interface velocity - solute segregation coefficient" relation, being unique for a specific alloy composition, is anticipated to be acquired in the two numerical schemes. The volume free energy densities of the liquid and solid phases in the Si-As system adopted by Steinbach et al. [20] for a linear phase diagram were directly utilized:

$$f_L = \frac{RT}{V_m} \{c_L \ln(c_L) + (1 - c_L) \ln(1 - c_L)\} \quad (19)$$

$$f_S = \frac{RT}{V_m} \left\{ c_S \ln(c_S) + (1 - c_S) \ln(1 - c_S) - c_S \ln(k_e) + (1 - c_S) \ln \left[\frac{1 + \frac{(T_m - T)}{m_e}}{1 + \frac{k_e(T_m - T)}{m_e}} \right] \right\} \quad (20)$$

Where T is the simulation temperature, T_m is the melting temperature of the pure Si, c_L and c_S are the phase concentrations of liquid and solid phases, k_e and m_e are the partition coefficient and the liquidus slope of the equilibrium phase diagram, V_m is the molar volume and R is the idea gas constant.

Fig. 2 shows the overall concentration profiles according to the phase-field simulations using the two different numerical schemes with different sets of interface widths (η) and permeabilities (P) (i.e., $\eta = \eta_{\text{atom}}$, $P = 2.5 \times 10^4 \text{ cm}^3/(\text{Js})$ in Fig. 2(a), $\eta = 10 \eta_{\text{atom}}$, $P = 1.0 \times 10^3 \text{ cm}^3/(\text{Js})$ in Fig. 2(b), and $\eta = 100 \eta_{\text{atom}}$, $P = 70 \text{ cm}^3/(\text{Js})$ in Fig. 2(c)).

Here η_{atom} is the atomic interface width δ_{atom} and

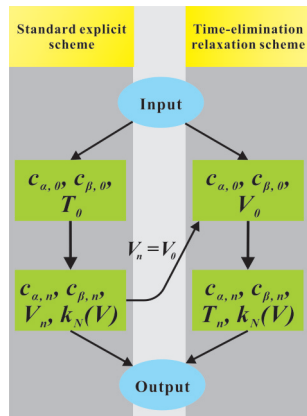


Figure 1. Flow chart of two different numerical schemes in the 1-D phase-field simulations of solute trapping in the Si-4.5 at.% As alloy during rapid solidification

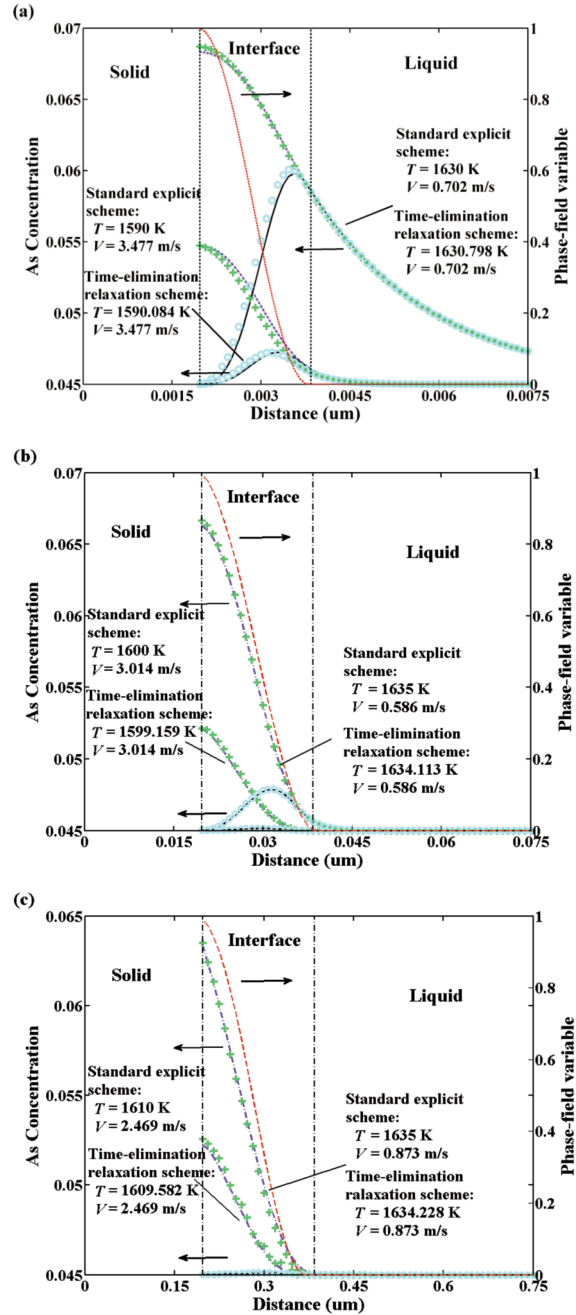


Figure 2. Phase-field simulated concentration profiles using two different phase-field schemes with different interface widths and interface permeabilities: (a) $\eta = 1.875 \times 10^{-7} \text{ cm}$, $P = 2.5 \times 10^4 \text{ cm}^3/(\text{Js})$, (b) $\eta = 1.875 \times 10^{-6} \text{ cm}$, $P = 1.0 \times 10^3 \text{ cm}^3/(\text{Js})$, (c) $\eta = 1.875 \times 10^{-5} \text{ cm}$, $P = 70 \text{ cm}^3/(\text{Js})$. The solid lines denote the overall concentrations, while the dotted lines the liquid concentrations due to the standard explicit scheme. Symbols represent the results due to the time-elimination relaxation scheme (\circ denotes the overall concentration, while $+$ the liquid concentration)

equals to $1.875 \times 10^{-7} \text{ cm}$, as shown in Table 1. The corresponding liquid concentration profiles are also displayed in the figures. As can be seen in the figures, under the steady state, the simulated concentration profiles from the two numerical schemes reach an ideal agreement over a wide range of interface velocities. Moreover, the overall concentration profile in the solid phase has a uniform value equal to the far-field concentration c_0 in the liquid under the steady state. The overall concentration increases in the interface region due to the rejection of solute atoms by the growing solid. In the liquid ahead of the interface, a concentration boundary layer forms due to the diffusive transport of the rejected solute atoms into the liquid. As temperature decreases and interface velocity increases, both maximum solute concentration and spatial penetration of the liquid concentration profile diminishes, which demonstrates an increase of solute segregation at the interface and an occurrence of the solute trapping. Additionally, it can be further found that the numerical interface width has also significant effect on the composition distribution. As the interface width increases, the maximum overall concentration and the range of concentration boundary layer decreases, which represents the extra solute trapping due to the part of the interface width in numerical simulation that exceeds the atomistic width.

Fig. 3 exhibits the relations between the interface velocity V and the temperature T due to the phase-field simulations of solute trapping in Si-4.5 at.% As during rapid solidification via both standard explicit scheme and time-elimination relaxation scheme with different sets of interface widths (η) and permeabilities (P). As shown in the figures, the interface velocity varies monotonically with the simulation temperature T . Moreover, the $V \sim T$ relations due to the two different simulation schemes are consistent with each other for different sets of interface widths (η) and permeabilities (P)

The predicted velocity-dependent solute segregation coefficients $k(V)$ for different sets of interface widths (η) and permeabilities (P) due to the phase-field simulations via the standard explicit and time-elimination relaxation simulation schemes are presented in Fig. 4(a). As shown in the figure, the predicted velocity-dependent solute segregation coefficients due to the two different numerical schemes are in reasonable agreement with each other. It can be further observed in Fig. 4(a) that the velocity-dependent solute segregation coefficient $k(V)$ generally increases as interface velocity increases, indicating the enhancement of the solute-trapping effect. Specifically, the decrease in the interface permeability P can noticeably enhance the solute-trapping effect, which is attributed to the decrease of the chemical partitioning process. Meanwhile, the

solute segregation coefficient can also be influenced as the interface widths changes. As demonstrated in references [20, 22], by adjusting η and P , the experimental solute segregation coefficients can be

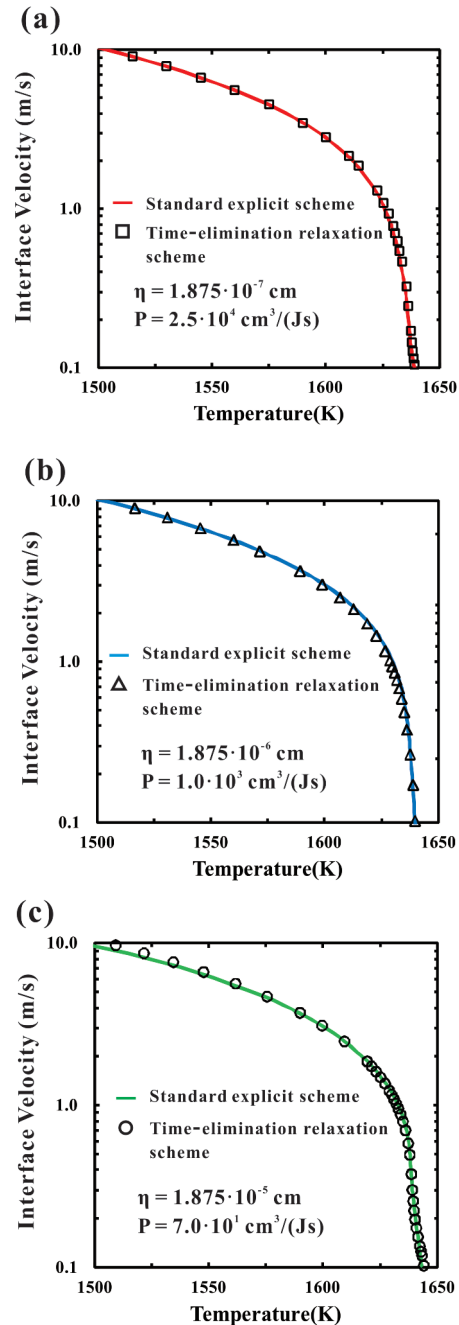


Figure 3. Phase-field simulated interface velocity as a function of temperature in the Si-4.5 at.% As alloy due to different numerical schemes with different interface widths: (a) $\eta = 1.875 \times 10^{-7} \text{ cm}$, (b) $\eta = 1.875 \times 10^{-6} \text{ cm}$, (c) $\eta = 1.875 \times 10^{-5} \text{ cm}$. Lines denote the results by the standard explicit scheme, while symbols denote those by the time-elimination relaxation scheme

well reproduced. The $k(V)$ curves based on the optimal set of interface width and the interface permeability via both standard explicit scheme and time-elimination relaxation scheme are plot in Fig. 4(b), compared with the experimental data from Kittl et al. [6]. As presented in this figure, the experimental data can be nicely reproduced by both standard explicit simulation scheme and time-elimination relaxation simulation scheme, which indicts the reliability of the present simulation.

On the basis of Fig. 3 and Fig. 4, it can be concluded that the phase-field model with finite interface dissipation can be used to simulate the rapid solidification process by using both standard explicit and time-elimination relaxation simulation schemes. With the same input, the same results can be obtained by using the two schemes without restriction to numerical length scale and interface velocity. Moreover, the convergence of the standard explicit scheme to the steady-state is very slow when the undercooling is low (that is, the interface velocity is low). By contrast, with the time-elimination relaxation scheme, the steady concentration distribution can be quickly acquired due to the elimination of temporal effect in the evolution equations. Therefore, for a 1-D simulation of rapid solidification in a target alloy using the phase-field model with finite interface dissipation, the time-elimination relaxation scheme is recommended. However, it should be also pointed out here that such a time-elimination relaxation scheme is not suitable for the future 3-D phase-field simulations of microstructure evolution during rapid solidification,

which can be described by the standard explicit numerical scheme.

What's more, kinetic phase diagram is a useful guidance to predict the phase concentrations at the target solidification velocity in industry design of new materials. According to the above discussion, both numerical schemes in the phase-field simulation can be applied to obtain kinetic phase diagram. For the standard explicit scheme, by adjusting the solidification temperature and initial alloy concentration, the solute segregation coefficient at a specific interface velocity, from which the kinetic phase diagram can be constructed, can be in principle predicted. However, the simulation process with the standard explicit scheme is numerical inefficient. While for the time-elimination relaxation scheme, with input of the fixed interface velocity and the varied initial alloy concentrations, the corresponding kinetic phase diagram can be easily acquired. Thus, the time-elimination relaxation scheme is used here to build the kinetic phase diagrams in the Si-As system. Fig. 5 illustrates kinetic phase diagrams of the Si-As system for different interface velocities based on the present phase-field simulation using the time-elimination relaxation scheme. In addition, the comparison with the equilibrium phase diagram of the Si-As system (i.e., V approaches to 0 m/s, denoted by solid lines) is also made in Fig. 5. The results show that the gap between liquidus and solidus gradually reduces as the interface moving velocity V increases, which demonstrates an occurrence of solute trapping and the tendency to diffusionless solidification.

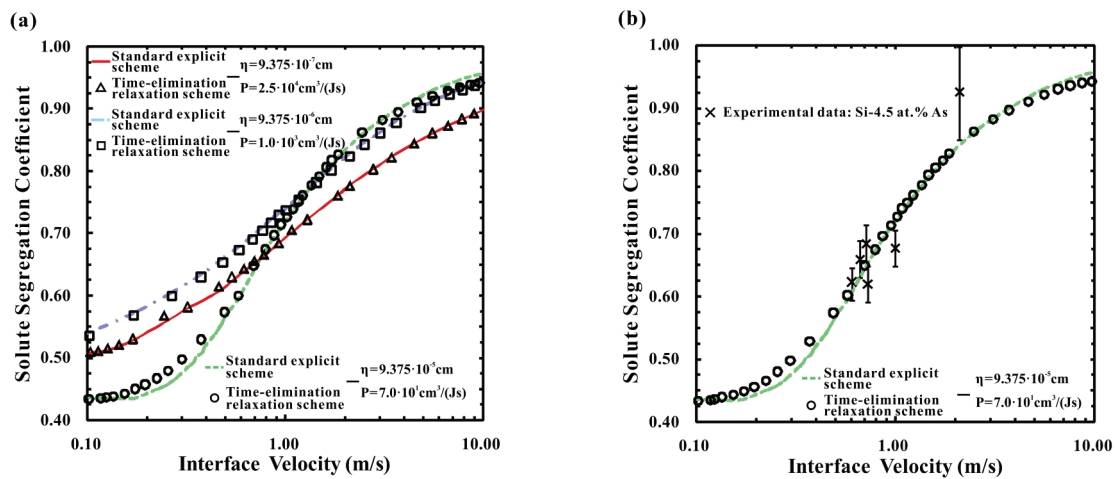


Figure 4. (a) Model-predicted solute segregation coefficients $k_s(V)$ as a function of the interface velocity in the Si-0.045 As alloy due to 1-D phase-field simulation using two different numerical schemes with different sets of interface widths and interface permeabilities. Lines denote the results by the standard explicit scheme, while symbols denote those by the time-elimination relaxation scheme. (b) Model-predicted solute segregation coefficients in the Si-0.045 As alloy due to the phase-field simulation using two different numerical schemes with the optimal interface width and interface permeability, compared with the experimental data from Kittl et al. [6]

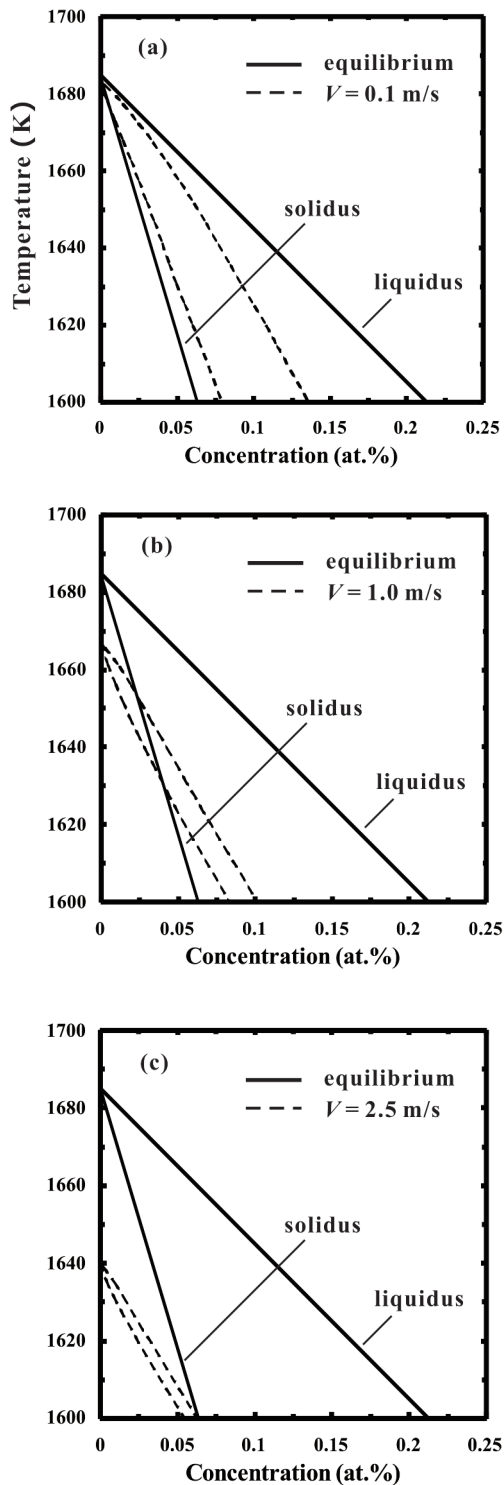


Figure 5. Model-predicted kinetic phase diagrams (dash lines) of the Si-As system at different interface velocities due to the 1-D phase-field simulation using the time-elimination relaxation scheme: (a) $V=0.1$ m/s, (b) $V=1.0$ m/s, (c) $V=2.5$ m/s. Solid lines represent the equilibrium phase diagram of the Si-As system

6. Conclusion

A comparative analysis of two different numerical schemes, the standard explicit scheme and the time-elimination relaxation scheme, in the framework of phase-field model with finite interface dissipation was performed by applying to investigate the solute trapping effect in a Si-4.5 at.% As alloy during rapid solidification. It was found that with the equivalent input, both numerical schemes can give the unique solute distribution. Moreover, the solute trapping phenomenon was nicely described, and the experimental solute segregation coefficients can be well reproduced with an optimal set of interface width and interface permeability. Based on a comprehensive analysis of advantages and disadvantages of the two numerical schemes, the time-elimination relaxation scheme was highly recommended for one-dimensional phase-field simulation of rapid solidification process. As for the future two- or three dimensional phase-field simulation, the standard explicit scheme might be the only choice. In addition, the technically important kinetic phase diagrams of the Si-As alloys were also predicted by using the one-dimensional phase-field simulation with the time-elimination relaxation scheme.

Acknowledgments

The authors would like to acknowledge financial support from National Natural Science Foundation for Youth of China under Grant No. 51301208, National Natural Science Foundation of China under Grant No. 51474239, Hunan Provincial Natural Science Foundation for Youth of China under Grant No. 2015JJ3146, Innovation Foundation For Postgraduate and Fundamental Research Funds of Central South University (Grant No. 2015zzts030), Changsha, People's Republic of China and the State Scholarship Fund from China Scholarship Council (No.201506370114). Lijun Zhang acknowledges support from Shenghua Scholar Program of Central South University, Changsha, P.R. China.

References

- [1] E. J. Lavernia, T. S. Srivatsan, *J. Mater. Sci.*, 45 (2010) 287-325.
- [2] J. C. Baker, J. W. Cahn, *Acta Metall.*, 17 (1969) 575-578.
- [3] W. Kurz, D. J. Fisher, *Fundamental of Solidification* Fourth ed., Switzerland, 1998, p.134-138.
- [4] P. M. Smith, M. J. Aziz, *Acta Metall. Mater.*, 42 (1994) 3515-3525.
- [5] M. J. Aziz, C. W. White, *Phys. Rev. Lett.*, 57 (1986) 2675-3678.
- [6] J. A. Kittl, M. J. Aziz, D. P. Brunco, M. O. Thompson, *J. Cryst. Growth*, 148 (1995) 172-182.

-
- [7] M. J. Aziz, *J. Appl. Phys.*, 53 (1982) 1158-1168.
- [8] M. J. Aziz, T. Kaplan, *Acta Metall.*, 36 (1988) 2335-2347.
- [9] S. L. Sobolev, *Phys. Lett. A*, 199 (1995) 383-386.
- [10] S. L. Sobolev, *Phys. Status. Solidi. A*, 156 (1996) 293-303.
- [11] P. K. Galenko, S. L. Sobolev, *Phys. Rev. E*, 55 (1997) 343-352.
- [12] P. K. Galenko, D. Danilov, *Phys. Lett. A*, 235 (1997) 271-280.
- [13] S. L. Sobolev, *Phys. Rev. E*, 55 (1997) 6845-6854.
- [14] S. L. Sobolev, *Tech. Phys.* 43 (1998) 307-313.
- [15] A. A. Wheeler, W. J. Boettinger, G. B. McFadden, *Phys. Rev. A*, 45 (1992) 7424-7439.
- [16] A. A. Wheeler, W. J. Boettinger, G. B. McFadden, *Phys. Rev. E*, 47 (1993) 1893-1909.
- [17] B. Nestler, A. A. Wheeler, *Phys. Rev. E*, 57 (1998) 2602-2609.
- [18] D. Danilov, B. Nestler, *Acta Mater.*, 54 (2006) 4659-4664.
- [19] V. G. Lebedev, E. V. Abramova, D. A. Danilov, P. K. Galenko, *Int. J. Mat. Res.*, 101 (2010) 473-479.
- [20] I. Steinbach, L. Zhang, M. Plapp, *Acta Mater.*, 60 (2012) 2689-2701.
- [21] L. Zhang, I. Steinbach, *Acta Mater.*, 60 (2012) 2702-2710.
- [22] L. Zhang, E. V. Danilova, I. Steinbach, D. Medvedev, P. K. Galenko, *Acta Mater.*, 61 (2013) 4155-4168.
- [23] X. Yang, L. Zhang, Y. Du, *Mater. Sci. Forum*, 794-796 (2014) 740-745.
- [24] I. Steinbach, F. Pezzolla, B. Nestler, M. Seeßelberg, R. Prieler, G. J. Schmitz, J. L. L. Rezende, *Physica D*, 94 (1996) 135-147.
- [25] J. Eiken, B. Böttger, I. Steinbach, *Phys. Rev. E*, 73 (2006) 066122.
- [26] I. Steinbach, *Annu. Rev. Mater. Res.*, 43 (2013) 89-107.
- [27] J. Tiaden, B. Nestler, H. J. Diepers, I. Steinbach, *Physica D*, 115 (1998) 73-86.
- [28] W. Chen, L. Zhang, Y. Du, C. Tang, B. Huang, *Scripta Mater.*, 90 (2014) 53-56.
- [29] J. Li, T. Liu, W. Chen, S. Wang, L. Zhang, Y. Du, H. Xu, *J. Min. Metall. Sect. B-Metall.* 50 (2014) 93-99.
- [30] O. Andersson, J. Ågren, *J. Appl. Phys.*, 72 (1992) 1350-1355.
- [31] L. Zhang, Y. Du, I. Steinbach, Q. Chen, B. Huang, *Acta Mater.*, 58 (2010) 3664-3675.
- [32] B. Vinet, L. Magnusson, H. Fredriksson, P. J. Desré, *J. Colloid Interface Sci.*, 255 (2002) 363-374.